Probing Individual Redox PEGylated Gold Nanoparticles by Electrochemical–Atomic Force Microscopy

Kai Huang, Agnès Anne, Mohamed Ali Bahri, and Christophe Demaille*

Laboratoire d'Electrochimie Moléculaire, UMR 7591 CNRS, Université Paris Diderot, Sorbonne Paris Cité, 15 Rue Jean-Antoine de Baïf, F-75205 Paris Cedex 13, France

ABSTRACT Electrochemical–atomic force microscopy (AFM-SECM) was used to simultaneously probe the physical and electrochemical properties of individual ~20 nm sized gold nanoparticles functionalized by redox-labeled PEG chains. The redox PEGylated nanoparticles were assembled onto a gold electrode surface, forming a random nanoarray, and interrogated *in situ* by a combined AFM-SECM nanoelectrode probe. We show that, in this so-called mediator-tethered (Mt) mode, AFM-SECM affords the nanometer resolution required for resolving the position of individual nanoparticles and measuring their size, while simultaneously electrochemically directly contacting the redox-PEG chains they bear. The dual measurement of the size and current response of single nanoparticles uniquely allows the statistical distribution in grafting density of PEG on the nanoparticles to be determined and correlated to the nanoparticle diameter. Moreover, because of its high spatial resolution, Mt/AFM-SECM allows "visualizing" simultaneously but independently the PEG corona and the gold core of individual nanoparticles. Beyond demonstrating the achievement of single-nanoparticle resolution using an electrochemical microscopy technique, the results reported here also pave the way toward using Mt/AFM-SECM for imaging nano-objects bearing any kind of suitably redox-labeled (bio)macromolecules.

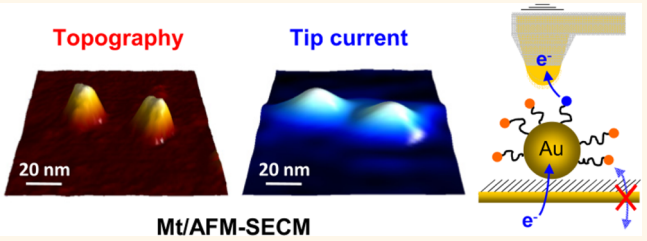

KEYWORDS: PEGylated gold nanoparticles · electrochemical microscopy · SECM · electrochemical–atomic force microscopy · AFM-SECM · mediator-tethered/electrochemical atomic force microscopy · Mt/AFM-SECM

Characterizing the physical and chemical properties of noble metal nanoparticles, either as isolated objects or forming nanostructures on surfaces, is a topic of current interest.[1] Gold nanoparticles have in particular attracted much attention, notably because they can easily be endowed with a vast range of functionalities *via* the self-assembly of layers of organic molecules and biomolecules onto their surface.[2−4] Gold nanoparticles can for example be functionalized by specific ligands, such as DNA strands[5,6] or peptide chains,[7] for chemical and biochemical sensing applications.[8] Functionalized gold nanoparticles have also found many applications in the emerging field of medical imaging and therapy.[9] For these applications, gold nanoparticles are typically protected from the immune system by a polyethylene glycol (PEG) coating.[9,10] Redox functionalities can also be incorporated into the layer coating the gold nanoparticles for their use as faradaic electron reservoirs for electrocatalysis;[11,12] these redox-functionalized nanoparticles can as well be adsorbed onto surfaces in view of making high charge storage devices.[13,14] No matter the targeted application, it is of course indispensable that the properties of the molecular coating of functionalized nanoparticles are fully characterized. Of particular interest is the assessment of the number of copies of the functional molecules introduced on the surface of the nanoparticles. So far such a characterization of the degree of functionalization of gold nanoparticles has been carried out using methods that only measure the average properties of samples containing a large number of nanoparticles.[4,11] However, these ensemble measurements inherently mask the disparity of the properties of the nanoparticles, which may display unique individual characteristics. Therefore, it is much desirable to develop techniques allowing the properties of functionalized nanoparticles, such as their degree of functionalization, to be quantified at the single-nanoparticle

* Address correspondence to demaille@univ-paris-diderot.fr.

Received for review January 31, 2013 and accepted April 7, 2013.

Published online April 07, 2013
10.1021/nn400527u

level. In addition, because the properties of nanoparticles are often size-dependent, such techniques should also allow the size of the particles to be determined jointly with their functional properties. Combined local probe microscopy techniques, offering single-nanoparticle resolution, uniquely fulfill these criteria[15] and have indeed been used to characterize bare gold nanoparticles,[16,17] but very rarely to study functionalized (or simply coated) gold nanoparticles. To the best of our knowledge only Abate *et al.* reported combined atomic force microscopy (AFM)/near-field scanning optical microscopy (NSOM) single-particle-level characterizations of silica[18,19] and surfactant-capped gold nanoparticles.[20]

The aim of the present work is to explore the possibility of using scanning electrochemical microscopy[21−23] (SECM), a spatially resolved *in situ* electrochemical technique using a microelectrode as a local probe, for characterizing *individual* redox-labeled gold nanoparticles.

Ever since a very early attempt by Bard *et al.*,[24] the ability to interrogate individual nanoparticles by SECM has remained an elusive goal. This limitation was initially due to the modest resolution of SECM, which, for a long time, has remained in the micrometer range.[21,22] Resolution has since been improved down to the submicrometer range by combining SECM with AFM, *via* the fabrication and use of submicrometer-sized AFM-SECM probes.[25−27] The recent development of hyphenated SECM techniques[28] and the production of nanoelectrodes usable as SECM local probes[29−32] have resulted in further resolution improvements, which, for example, allowed Amemiya *et al.* to succeed in probing nanoband electrodes,[33] nanogaps,[34] or single-wall nanotubes[35] by SECM. Unwin *et al.* also probed the reactivity of single-wall nanotubes[36] and of isolated ∼100 nm sized catalyst particles[37] using scanning electrochemical cell microscopy (SECCM), a SECM-derived technique they designed.[38] Most recently, using the same technique, this later group succeeded in probing the reactivity of 10−15 nm sized single bare gold nanoparticles.[39] Yet the actual size of the particles probed had to be measured *ex situ* by TEM. It is also worth mentioning that, very early on, Stimming *et al.* made use of scanning tunneling microscopy (STM), operated in an SECM-resembling configuration, to probe the electrochemical reactivity of bare, single ∼10 nm sized palladium nanoparticles.[40] However, to date no actual electrochemical technique exists allowing the *simultaneous* measurement of the size of nanoparticles and the probing of their redox properties.

In that context, we propose here to use a high-resolution variant of SECM, which we introduced earlier and labeled Mt (mediator-tethered)/AFM-SECM,[41−43] for probing individual nanoparticles functionalized by redox-labeled macromolecules. The principle of Mt/AFM-SECM is that a force-sensing microelectrode probe is used to directly contact redox-labeled macromolecules immobilized onto a conducting substrate. Electrochemical detection of the redox label generates a *specific* tip current, whose intensity depends on the *local* surface concentration of the redox macromolecule on the surface.[41,42] When operated in imaging (tapping) mode, Mt/AFM-SECM allows the surface distribution of the redox-labeled macromolecule to be mapped, while the topography of the substrate is simultaneously acquired.[43,44] We previously demonstrated that Mt/AFM-SECM could be used to electrochemically interrogate nanometer-sized linear macromolecules, such as PEG[41−43] or short DNA chains,[45] end-attached to a surface, and also to map the surface distribution of ∼100 nm sized immunocomplex dots.[44]

In the work reported herein, Mt/AFM-SECM is used to image a random array of ∼20 nm sized gold nanoparticles functionalized by a molecular layer of nanometer-sized polyethylene glycol $(PEG)_{3400}$ chains end-labeled by a redox (ferrocene, Fc) group. We show that the Mt/AFM-SECM configuration allows locating individual Fc-PEGylated nanoparticles, measuring their size, and simultaneously electrochemically interrogating the Fc-PEG molecules they bear. We demonstrate that these measurements uniquely allow accessing the statistical distribution of Fc-PEG grafting density on the nanoparticles, a parameter that had remained inaccessible to the "ensemble" techniques so far used to characterize PEGylated particles,[46,47] and cross-correlating the nanoparticle coverage and sizes.

RESULTS AND DISCUSSION

Assembly of a Random Gold Nanoparticle/Nanoelectrode Array. A natural prerequisite for studying nanoparticles by local probe techniques is that the particles are immobilized on a planar surface. In the present case, where we aim at probing gold nanoparticles functionalized by Fc-PEG chains, we had the choice of functionalizing the nanoparticles by Fc-PEG either before or immediately following their immobilization on the surface. We preferred the later strategy since we feared that the repelling properties of the PEG layer would hamper proper attachment of the functionalized particles to the surface. Hence the first experimental step was to form an array of *bare* gold nanoparticles on a surface, with the additional constraint that, to enable the electrochemical detection of the redox-labeled PEG chain, the nanoparticles had to act as individual nanoelectrodes. Our experimental approach, for the construction of such a nanoparticle/nanoelectrode array, is based on the recent reports by Gooding *et al.*[48,49] These authors demonstrated that citrate-stabilized gold nanoparticles adsorbed onto amine-terminated alkyl thiols self-assembled onto gold electrodes were able to mediate charge transfer from the

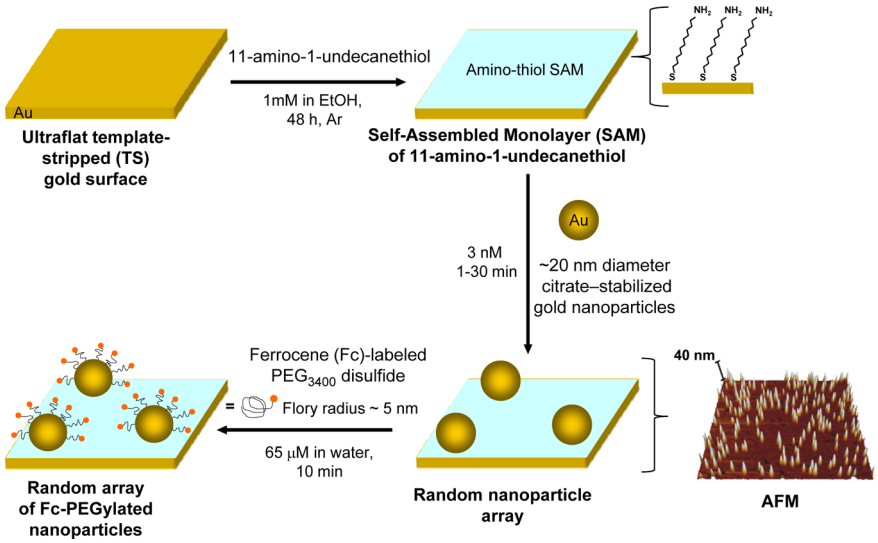

Figure 1. Fabrication of a random array of Fc-PEGylated gold nanoparticles on a gold surface. The AFM image shown is a 3 μm × 3 μm tapping mode topographic image of a random nanoparticle array acquired in air using a commercial AFM probe. Nanoparticle surface coverage as derived by particle counting from the AFM image: $\gamma \approx 60$ particles/μm^2.

underlying gold electrode toward redox species in solution. They showed that gold nanoparticles could transport electrons across thick self-assembled layers of alkyl amino-thiols, which in the absence of nanoparticles would otherwise fully passivate the gold electrode surface. This paradoxical electrochemical property, first observed by Natan *et al.*,[50] further described by Brust et *al.*,[51] and thoroughly studied by Fermín *et al.*[52] for various types of electrode−monolayer−nanoparticle constructs, has been recently rationalized on a theoretical basis by Chazalviel *et al.*[53]

In the present work, a compact layer (SAM) of a long amino alkyl thiol molecule, 11-amino-1-undecanethiol, was first assembled onto an ultraflat template-stripped (TS) gold surface (see Figure 1).

The quality of the amino-thiol layer and its passivating properties were confirmed by the observation that the electrochemical signal of the soluble redox species ferrocene dimethanol at the gold surface was almost entirely suppressed following SAM assembly (see Supporting Information). Ferrocene methanol was chosen as a test redox species due to its chemical identity with the Fc label of the PEG chains used here.

Citrate-stabilized gold nanoparticles ~20 nm in diameter were then adsorbed onto the amino-thiol layer by immersing the SAM-modified gold surface into the nanoparticle-containing solution. The ensuing formation of electrostatic and probably partly covalent bonds between the nanoparticles and the amino functionalities of the SAM resulted in the assembly of a robust nanoparticle array (see Figure 1). The presence of nanoparticles onto the surface was verified by AFM microscopy imaging in air, which also served to determine the nanoparticle surface coverage by counting the particles visible in 3 μm × 3 μm topographic images (see Figure 1). The ability of the gold nanoparticles to shuttle electrons, *i.e.*, to act as nanoelectrodes, was confirmed by cyclic voltammetry experiments, which showed that the signal of ferrocene dimethanol was fully restored after adsorption of the gold nanoparticles onto the SAM (see Supporting Information).

We also used AFM imaging to find the experimental conditions allowing the surface coverage of nanoparticles on the SAM-modified substrates to be finely tuned. Controlling the interparticle separation was of great importance here since we wanted the nanoparticles to be sufficiently spaced apart in order to be individually addressable by the finite-sized Mt/AFM-SECM tip. We found that exposing the SAM-bearing gold surface to a 3 nM nanoparticle solution for 1−10 min allowed us to reproducibly obtain random arrays characterized by a nanoparticle surface coverage of $\gamma = 20-150$ particles/μm^2, *i.e.*, by an average nanoparticle separation of ~0.1−0.25 μm.

Hence the random nanoparticle array fabricated here displays two important features for its use as a platform allowing the Mt/AFM-SECM characterization of Fc-PEGylated particles: The SAM matrix is sufficiently insulating to prevent direct electrochemistry of Fc species at the gold surface and electrochemical detection of Fc species at the nanoparticle is, oppositely, unhindered and fast.

Directed Immobilization of Fc-PEG Chains onto the Gold Nanoparticles. Determining the Average Number of Fc-PEG Chains per Nanoparticle by Cyclic Voltammetry. Immobilization of the Fc-PEG chains was selectively directed to the gold nanoparticles by exposing the surfaces bearing nanoparticle arrays to an aqueous solution of a custom-synthesized Fc-PEG$_{3400}$-disulfide molecule.[59]

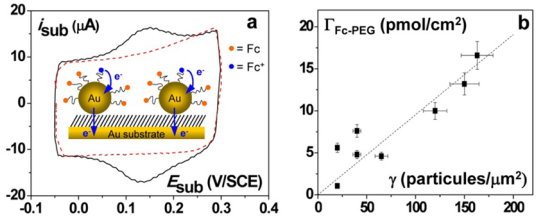

Figure 2. (a) Cyclic voltammograms recorded at a TS-gold surface bearing ~20 nm citrate-stabilized gold nanoparticles adsorbed on a self-assembled monolayer of 11-amino-1-undecanethiol. The voltammograms were recorded before (dashed trace) and after (continuous trace) functionalization of the surface-adsorbed nanoparticles by Fc-PEG-disulfide. (b) Overall surface coverage in Fc-PEG chains, Γ_{Fc}, as determined by cyclic voltammetry for various TS surfaces bearing Fc-PEGylated nanoparticles, as a function of their respective nanoparticle coverage, γ. In (a), scan rate = 2 V/s, electrolyte = aqueous 0.1 M citrate buffer pH 6.

This molecule was selected for several reasons: (i) PEGylated nanoparticles used for biomedical applications are typically functionalized with PEG chains of similar molecular weight (in the 1−10 kD range).[9] (ii) The ferrocene (Fc) end-label of the chain displays an ideal electrochemical behavior.[43] (iii) Finally, the high affinity of disulfide for gold is expected to result in the end-grafting of Fc-PEG chains onto the gold nanoparticles (Figure 1), just as what has been observed to occur at planar gold surfaces.[43] Actual immobilization of the Fc-PEG chains on the array was monitored by cyclic voltammetry (CV): Figure 2a shows the voltammograms recorded at a nanoparticle array substrate before (dashed trace) and after (continuous trace) 10 min exposure of the nanoparticle-modified substrate to a 65 μM Fc-PEG-disulfide aqueous solution.

One can observe that the voltammogram recorded after the Fc-PEG-disulfide treatment changes from being purely capacitive into the typical reversible peak-shaped signal expected for a surface-confined species undergoing fast (Nernstian) electron transfer with the surface.[54] The peak-to-peak separation is very small (less than ~10 mV at 2 V/s), and the intensity of the current peaks increases linearly with scan rate. Importantly, the peak width at mid height is ~110 mV, which is reasonably close to the value of 90 mV expected for a homogeneous population of noninteracting surface-bound redox species located outside the double layer. Finally, the signal is centered around a potential of ~+0.14 V/SCE, which is close to the value of +0.15 V/SCE we determined earlier for the standard potential ($E^{\circ}_{Fc/Fc+}$) of the PEG-borne Fc/Fc^{+} redox couple, either free in solution or attached to gold electrodes or biomolecular surfaces.[41,44] These results indicate that, as schematized in Figure 2a, the Fc heads can reversibly exchange electrons with the underlying gold substrate *via* the nanoparticles on which they are anchored. Integration of the background-subtracted CV signal yields the *overall* surface coverage in Fc-PEG chains, Γ_{Fc} (in moles per geometric substrate surface area). For the various substrates we examined, all bearing Fc-PEGylated nanoparticles, but differing in their nanoparticle surface coverage γ, we measured Γ_{Fc} values ranging from 1 to 17 pmol/cm^2. Strikingly, we observed that the value of Γ_{Fc} varied *linearly* with the value of γ (see Figure 2b). This result confirms that the Fc-PEG chains are borne by the nanoparticles and allows n_{av}, the *average* number of Fc-PEG chains per nanoparticle, to be determined by linear regression of the Γ_{Fc} *vs* γ variation, yielding $n_{av} = 550 \pm 200$. We also observed that, for any given surface, Γ_{Fc} did not increase further when the SAM/nanoparticle/Fc-PEG-bearing surface was reimmersed into the Fc-disulfide solution, indicating that the Γ_{Fc} and n_{av} values measured here correspond to saturation of the surface of the nanoparticles by the PEG chains. Importantly we verified as well, by measuring γ both before and after immersion of the surface in the PEG-disulfide solution, that PEGylation of the nanoparticles did not result in any noticeable nanoparticle loss from the surface.

As further, definitive, evidence that the Fc-PEG chains are indeed borne by the nanoparticles and not inserted into the SAM matrix, we designed a blank experiment where an amino SAM-modified electrode, not bearing nanoparticles, was left in contact with the Fc-PEG-disulfide solution for increasing amounts of times and then interrogated by cyclic voltammetry. We observed that for the short contact times we used here (of less than an hour), no inserted Fc-PEG chains were detectable (see Supporting Information). Insertion of Fc-PEG chains into the SAM matrix did ultimately occur, but only for contact times longer than a few hours.

Ever since PEG-modified gold nanoparticles were first described by Murray *et al.*,[10] the issue of reliably measuring the average grafting density of PEG on nanoparticles has been debated[2,46] and has been very recently revisited.[46,47] The voltammetry results obtained here for our nanoparticle/Fc-PEG system are thus worth discussing further in that respect. For comparing our results with data from the literature, we first convert n_{av} into the so-called grafting density of Fc-PEG on the nanoparticles, defined as the number of PEG chains per unit surface area of the nanoparticle, which, considering spherical 15−20 nm diameter nanoparticles, is $\sim n_{av}/\pi(15-20)^2 \approx 0.4-0.8$ PEG chain/nm^2. We note that this latter value is significantly lower than grafting densities reported for PEGylated gold nanoparticles dimensionally similar to ours, but dispersed in solution. For example a PEG grafting density of 1.6 PEG/nm^2 was reported for PEG_{2000} chains thiografted onto 42 nm diameter citrate-stabilized gold nanoparticles.[46] Similarly, attachment of thiolated PEG_{2000} and PEG_{5000} chains onto 10 nm diameter citrate-stabilized gold nanoparticles was reported to result in grafting density values of 2.5 and 1.8 PEG/nm^2, respectively.[47] Hence from these figures one would

have expected to find about 1400−2500 chains borne by the ∼15−20 nm diameter gold nanoparticles used here (taking ∼2 PEG/nm^2). A reduced accessibility of surface-attached nanoparticles, as opposed to nanoparticles in solution, may partly explain this discrepancy. We note however that the average PEG grafting density we measured is significantly higher than the one we determined previously for Fc-PEG$_{3400}$ chains grafted onto planar surfaces. In such a case a saturating density of ∼0.1 chain/nm^2 was consistently measured.[43] This low grafting density value indicated the formation of dilute Fc-PEG layers onto planar surfaces, within which the end-grafted PEG chains adopted a hemispherical (so-called mushroom) conformation characterized by a Flory radius, R_F, of ∼5 nm. The fact that the *same* Fc-PEG molecule is now observed to form a much denser layer on a nanoparticle surface illustrates particularly clearly the effect of the curvature of the grafting interface on the surface density of polymers. This phenomenon is rooted to the fact that, as predicted by the Daoud−Cotton model[55] and confirmed by simulations,[56,57] polymer chains end-grafted onto curved interfaces can form high-density spherical brushes where the chain monomers occupy a conical section extending radially from the surface. This effect of the curvature of the grafting interface is theoretically expected to arise when the radius of the anchoring surface (particle), R_{NP}, is much smaller than the Flory radius of the chains, R_F.[56] However our experimental results suggest that even for a modest R_{NP}/R_F ratio of ∼1.5−2, characterizing our present system, transition from a mushroom regime to a spherical brush regime is noticeable.

Mt/AFM-SECM Characterization of Individual Fc-PEGylated Nanoparticles. A home-fabricated combined AFM-SECM probe,[64] capable of acting both as a tapping mode AFM probe and as a conical microelectrode, was excited at its resonance frequency (located in the 2−3 kHz region) and approached *in situ*, in a 0.1 M pH 6 citrate buffer solution, from surfaces bearing a low-density Fc-PEGylated nanoparticle array. The combined probe (tip) was biased at a potential of $E_{tip} = +0.3$ V/SCE, while a potential of $E_{sub} = -0.1$ V/SCE was applied to the surface (substrate). When a predefined (∼15%) damping of the tip oscillation amplitude was reached, the approach stopped and the tip was scanned along the surface. The surface topography and tip current signals were simultaneously acquired during the scan, and the corresponding images are respectively shown in Figure 3a and Figure 3b.

Examination of the topography image reveals a very flat surface, bearing a few (∼10) nano-objects characterized by a height in the 15−20 nm range and a width around ∼80 nm (see cross section of the topography image). These objects are naturally attributed to gold nanoparticles, since their height falls in the expected size range of the nanoparticles used here.

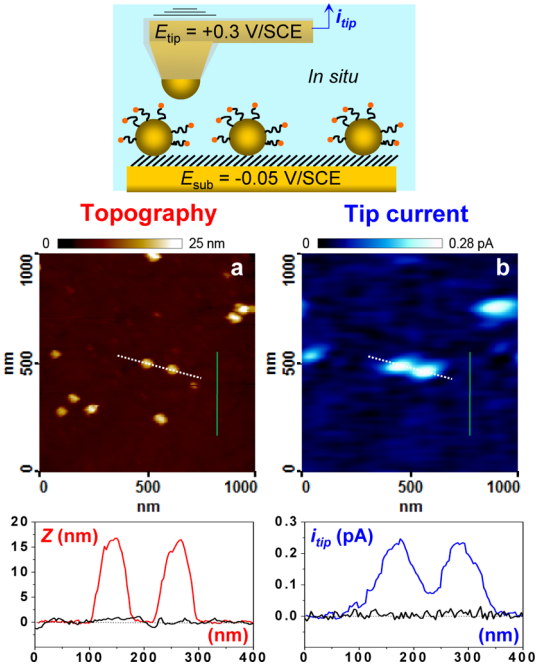

Figure 3. Mt/AFM-SECM tapping mode imaging of a gold surface bearing a random array of ∼20 nm Fc-PEGylated gold nanoparticles. Simultaneously acquired topography (a) and tip current images (b). Cross sections of the topography and current images taken along the short white line shown, passing through the center of two nanoparticles, are respectively plotted in red and blue. Corresponding cross sections taken in a zone free of nanoparticles, materialized by a vertical green line in the images, are plotted as black traces. Tip and substrate potentials: $E_{tip} = +0.30$ V/SCE, $E_{sub} = -0.05$ V/SCE. The probe is oscillated at its fundamental flexural frequency of 2.41 kHz, ∼15% damping, imaging rate 0.4 Hz, aqueous 0.1 M citrate buffer pH 6.

The relatively large apparent width of the nanoparticles, with respect to their height, can be explained by tip convolution effect, a well-known artifact in AFM imaging causing an overestimation of the dimension of objects imaged by a finite-sized AFM tip. In the case of a spherical tip of radius R_{tip} imaging a spherical object of radius R_0, the apparent object width of the object, W, is given by $W = 4(R_{tip}R_0)^{1/2}$.[58] Hence in the present case considering that the diameter of the homemade AFM-SECM probe used to acquire the images presented in Figure 3 was ∼100 nm, a ∼15−20 nm sized nanoparticle is expected to display an apparent width of $W \approx 80-90$ nm, in agreement with what can be measured in Figure 3a. This result confirms that individual nanoparticles, rather than clusters of particles, are visible in Figure 3.

Turning now to the current image, Figure 3b, we see that some of the nanoparticles visible in the topography image can be associated with a current "spot" in the current image, whereas others do not give rise to any current. On average we observed that 70−80% of the particles were "active" (*i.e.*, generated a current), whereas the rest were "inactive". Incidentally the fact that some particles, well resolved in the topography

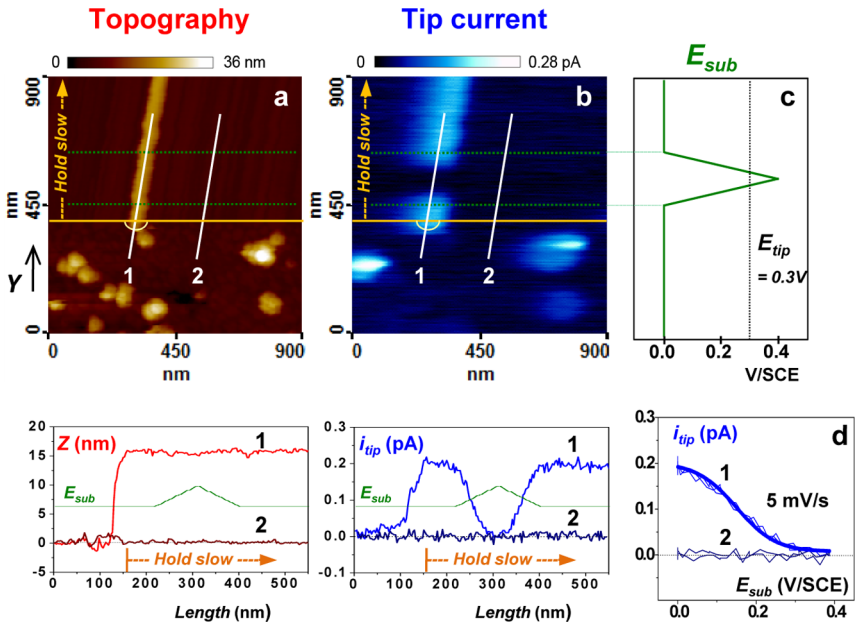

Figure 4. Mt/AFM-SECM tapping mode imaging of a gold surface bearing a random array of ~20 nm Fc-PEGylated gold nanoparticles. Simultaneous acquired topography (a) and tip current images (b). The images were acquired to evidence the dependence of the tip current, i_{tip}, on the substrate potential, E_{sub}. Plots of the cross section of the topography and current images taken along the white lines labeled 1 and 2 are shown below the corresponding images. The images were acquired from bottom to top. At some point of the scan, indicated by orange lines both in the images and in the cross section plots, the scanning mode was changed to "hold-slow"; that is, the same line of the image was scanned repeatedly. Later on, when the scan reached the position indicated by green dotted lines in the current image, E_{sub} was linearly swept to +0.4 V/SCE and back at 5 mV/s. This potential sweep is represented in (c) and is also superimposed to the cross section plots (green trace). In (d) the tip current, measured along the cross section of 1 and 2, is plotted as a function of the corresponding substrate potential. E_{tip} = +0.30 V/SCE; E_{sub} is initially set to 0.0 V/SCE. The probe was oscillated at its fundamental flexural frequency of 2.40 kHz, with ~20% damping. The imaging rate was 0.4 Hz in the lower part of the image and 0.2 Hz in the upper (hold-slow) part. Aqueous 0.1 M citrate buffer pH 6.

image, did not give rise to any current ascertains the absence of cross-talk between the topography and current signals. In order to check if the absence of current at the level of inactive particles could be due to a poor electrical connection of those particles with the underlying surface, we conducted conducting AFM experiments in air. These experiments consisted in imaging a SAM/nanoparticle-bearing substrate using a conductive commercial probe while applying a small bias between the tip and substrate. The simultaneously obtained topography and current images allowed us to demonstrate that virtually all (~90%) of the nanoparticles were effectively in electrical contact with the gold substrate (see Supporting Information). Such a result indicates that even "inactive" particles are in proper electrical contact with the substrate.

One can also see from Figure 3b that absolutely no current is recorded in the flat regions of the surface separating the nanoparticles. In contrast, as can be measured from the cross section of the current image, a current on the order of 0.2−0.3 pA is recorded at the level of the "active" nanoparticles. Importantly the images shown in Figure 3 could be repeatedly acquired, showing that the interaction between the homemade AFM-SECM probe and the nanoparticles was gentle enough not to damage the nanoarray surface.

In order to gain insights into the origin of the current recorded at the level of the "active" particles, the dependence of the tip current on the potential applied to the substrate was studied. To do so, a substrate bearing a Fc-PEGylated nanoparticle array was initially imaged in tapping mode Mt/AFM-SECM as described above, until a nanoparticle associated with a tip current was found, at which stage the "slow" (*Y*) scan direction was disabled (see Figure 4). In this so-called "hold-slow mode", the probe was thus endlessly scanned over the same nanoparticle while the topography and current signals were recorded and plotted as scan lines of the corresponding images.

Consequently the nanoparticle and its associated current signal appear as "bands" in the topography and current images (Figure 4a and b). The fact that the bands are inclined is due to a slow surface drift in the right-hand-side direction. This drift is particularly visible in the hold-slow mode since the scan rate was decreased from 0.4 line/s down to 0.2 line/s for a better accuracy of the current measurement. However this drift can be exactly compensated by considering cross sections of the images taken along the axis of the inclined bands, such as the cross section labeled 1 in the images presented in Figure 4. For the sake of comparison a cross section, labeled 2 in Figure 4, was

taken in a featureless region of the images. These topography and current cross sections are plotted in the lower part of Figure 4; the horizontal orange dashed lines denote the position where the hold-slow mode was activated. One can see upon examining cross section 1 that before the hold-slow mode was enabled the tip progressively "climbed" over the ~16 nm high nanoparticle, while the current increased concomitantly. Once the hold-slow mode was enabled, both the topography and the current signals remained approximately constant. At some point of the scan, indicated by green dotted lines in the current image and in its cross section, the substrate potential, E_{sub}, was ramped linearly with time toward anodic values and back to its initial value (see Figure 4c). One can see that such a ramp resulted in a black "ditch" in the current band visible in Figure 4b. This phenomenon can be more clearly seen by considering the current cross section, where the substrate potential, E_{sub}, is plotted as a green trace and superimposed to the tip current signal. One can see that as the value of E_{sub} is made more anodic, the tip current, i_{tip}, decreases progressively to zero, but is fully restored upon ramping E_{sub} back to its initial value of −0.05 V/SCE. If one now plots the measured value of i_{tip} as a function of the set E_{sub} value, the i_{tip} *vs* E_{sub} variation shown in Figure 4d is obtained. This S-shaped variation is typical of an electrochemical process probed by a microelectrode. Moreover its potential at midheight is found to be 0.17 V/SCE, a value close to the standard potential of the Fc/Fc^+ PEG borne redox couple (~0.15 V/SCE). This latter result demonstrates without any ambiguity that what has been achieved here is probing of the electrochemical response of Fc-PEG chains borne by *individual* gold nanoparticles.

As schematized in Figure 5, the Fc heads of the Fc-PEG borne by individual gold nanoparticles are alternatively oxidized at the tip and reduced back at the nanoparticle, which acts both as a scaffold and as a nanoelectrode. The resulting electrochemical tip current is kinetically controlled by the dynamics of the PEG-chain motion.[41] But what is most important here is that the tip current is proportional to the number of PEG-chains contacted by the tip, which depends linearly on the surface coverage of Fc-PEG on the nanoparticles.[42,43]

Hence, at this stage, we demonstrated here that tapping mode Mt/AFM-SECM uniquely allows the location of individual nanoparticles to be resolved while the PEG chains they bear are simultaneously electrochemically interrogated.

To the best of our knowledge this is the first example of an SECM-derived technique allowing the size and the electrochemical properties of individual, nanometer-sized objects to be simultaneously probed. Incidentally this result also demonstrates the capability of Mt/AFM-SECM for resolving the 2D distribution of

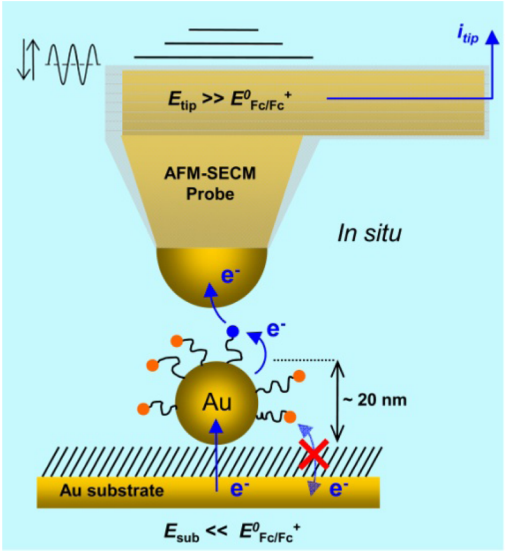

Figure 5. Principle of the Mt/AFM-SECM electrochemical interrogation of Fc-PEG chains here borne by individual gold nanoparticles. The nanoparticle acts both as a scaffold and as a nanoelectrode, mediating electron transfer between the underlying gold substrate and the redox (Fc) labels of the PEG. The AFM-SECM probe (tip) is brought *in situ* in "molecular" contact with the macromolecular PEG layer covering the nanoparticle. The tip and substrate are biased so that the redox label is alternatively oxidized at the tip and rereduced at the substrate. This redox cycling generates a *specific* tip electrochemical current whose intensity depends on the (time-averaged) tip−substrate distance, the Brownian dynamics of the PEG, and the local surface concentration in PEG. The use of tapping mode allows the tip−substrate distance to be fixed so that the tip current *specifically* probes the presence of the labeled molecule and its surface concentration (coverage) on the nanoparticle.

redox-labeled macromolecules down to a ~20 nm resolution.

Of particular interest is also the fact that what is actually measured here is the coverage of PEG chains on *individual* nanoparticles. So far, this important parameter has been accessible only as an average number derived from ensemble measurements, such as in our case cyclic voltammetry measurements at the substrate (see above). In that respect the absence of tip current at the level of the "inactive" nanoparticles has to be interpreted as the absence of Fc-PEG chains on those particles.

Imaging High-Density Fc-PEGylated Gold Nanoparticle Layers. Probing the Distribution of the Topographical and Electrochemical Properties of the Nanoparticles. The interest of the "nano-array"-like format in which the Fc-PEGylated nanoparticles are studied here is that, simply by imaging such an array, a large number of nanoparticles can be individually interrogated by the Mt/AFM-SECM probe in a single image scan, and the dispersion of the nanoparticle properties revealed. Of course this requires both a high nanoparticle coverage on the surface and a sharp enough AFM-SECM probe. We thus selected handmade AFM-SECM probes characterized

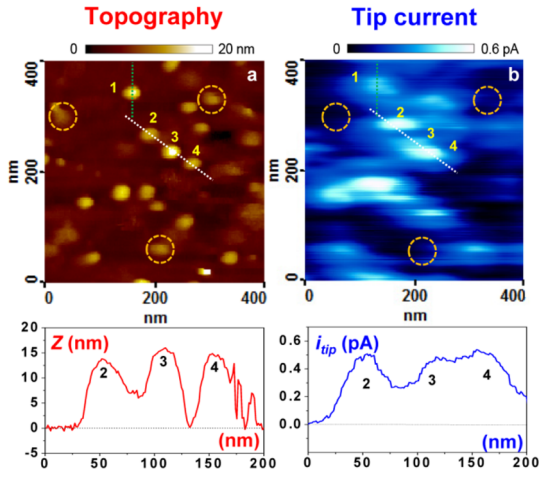

Figure 6. Mt/AFM-SECM tapping mode imaging of a gold surface bearing a high-density random array of ~20 nm Fc-PEGylated gold nanoparticles ($\gamma \approx 150$ particles/μm^2). Simultaneously acquired topography (a) and tip current images (b). Three "inactive" particles are circled. Cross sections of the topography and current images along the short white line shown, passing through the center of nanoparticles 2, 3, and 4, are presented below their corresponding images. The vertical green line passing through particle 1 denotes the position where the cross sections plotted in Figure 8 were taken. Tip and substrate potentials: E_{tip} = +0.30 V/SCE, E_{sub} = −0.05 V/SCE. The probe was oscillated at its fundamental flexural frequency of 2.28 kHz, with ~20% damping. Imaging rate 0.4 Hz. Aqueous 0.1 M citrate buffer pH 6.

by a tip radius in the ~20 nm size range, produced following a recently improved process (see Supporting Information), to image high-density Fc-PEGylated nanoparticle surfaces, characterized by a nanoparticle coverage in the order of $\gamma \approx 150$ particles/μm^2. Representative topography and current Mt/AFM-SECM images of such a surface are presented in Figure 6.

One can see from the topographic image, and corresponding cross section, that an immediate benefit of using a very sharp AFM-SECM probe is that the width of the nanoparticles is now ~40 nm, which is much closer to their actual diameter than previously. The thus minimized, but unavoidable, tip convolution effect allows a tip radius of 19 nm to be derived from the analysis of the topography image presented in Figure 6, proceeding as described above. Another benefit of using a sharp tip is that closely spaced nanoparticles, such as the particles labeled 2 and 3, or 3 and 4, which are only respectively 60 and 50 nm apart, can be clearly individually resolved (see cross section of the topography image). By measuring the height of the nanoparticles, the diameter of each of the nanoparticles visible in the image can be measured, and the particle size histogram presented in Figure 7a constructed. One can see that the nanoparticle size distribution is relatively broad and characterized by an average particle diameter of 15 nm and a standard deviation of 2.4 nm.

Turning now to the current image, we see that, as previously, some of the nanoparticles give rise to a clear current "spot". One can also note that the current spots tend to be elongated in the tip-scan (horizontal) direction. This current tailing effect is due to the slow rise and decay time of the low current measuring device. In spite of this, as seen from the current cross section shown in Figure 6, the individual tip current signals of the closely spaced nanoparticles, such as particles 2 and 3, and to a lesser extent 3 and 4, can be clearly resolved. The presence of a few "inactive" nanoparticles can also be noted: for the particular images presented in Figure 6 only 16 out of the 19 particles visible on the topography image seemed "active". It is also obvious that the color (*i.e.*, the intensity) of the current spots associated with the various "active" nanoparticles differs from one particle to the other As discussed above, this illustrates the fact that the degree of PEGylation varies from one particle to the other. This distribution in Fc-PEG coverage of the nanoparticles can be better visualized, and quantified, by constructing tip current histograms such as the one presented in Figure 7b.

One can see that, among the active nanoparticles, the distribution of tip current is essentially peak-shaped and centered around 0.45−0.5 pA/nanoparticle, a few particles giving rise to a tip current as low as 0.25 pA. Since the Fc-PEGylation of the nanoparticles was carried out in "saturating" conditions, *i.e.*, by exposing the nanoparticles to a Fc-PEG-disulfide solution for a long enough time for a maximal (saturating) Fc-PEG coverage to be reached, one might suspect that the tip current distribution is actually at least partly controlled by the nanoparticle size distribution. Hence we searched for a nanoparticle size/tip current correlation by plotting the intensity of the tip current generated by each nanoparticle as a function of the diameter of the *same* particle. Being able to establish such a cross-correlation between distinct properties of the same single nano-object is a unique benefit of the combined nature of the high-resolution Mt/AFM-SECM technique. The resulting plot, shown in Figure 7c, does not evidence any correlation between the nanoparticle size and tip current. Incidentaly, this result confirms that what is probed by the tip is the surface coverage of Fc-PEG chains on the nanoparticles and not the total amount of chains present on each particle, which scales as the square of the particle diameter. Nevertheless the distribution of the *number* of PEG chains per nanoparticle can be estimated as follows. The number of PEG chains, n_j, borne by a given particle j, is given by the product of Γ_j, the coverage in Fc-PEG chains of this particle, times the (spherical) nanoparticle surface, *i.e.*, $n_j = \pi d_j^2 \Gamma_j$ where d_j is the diameter of the particle. Considering that for the Mt/AFM-SECM technique the tip current i_j is proportional to Γ_j, *i.e.*, $I_j = \Gamma_j/\beta$, where β is a constant, we also have $n_j = \pi\beta i_j d_j^2$. By virtue of this equation we see that the average value of the $i_j \times d_j^2$ product, id^2, which can be estimated by considering all

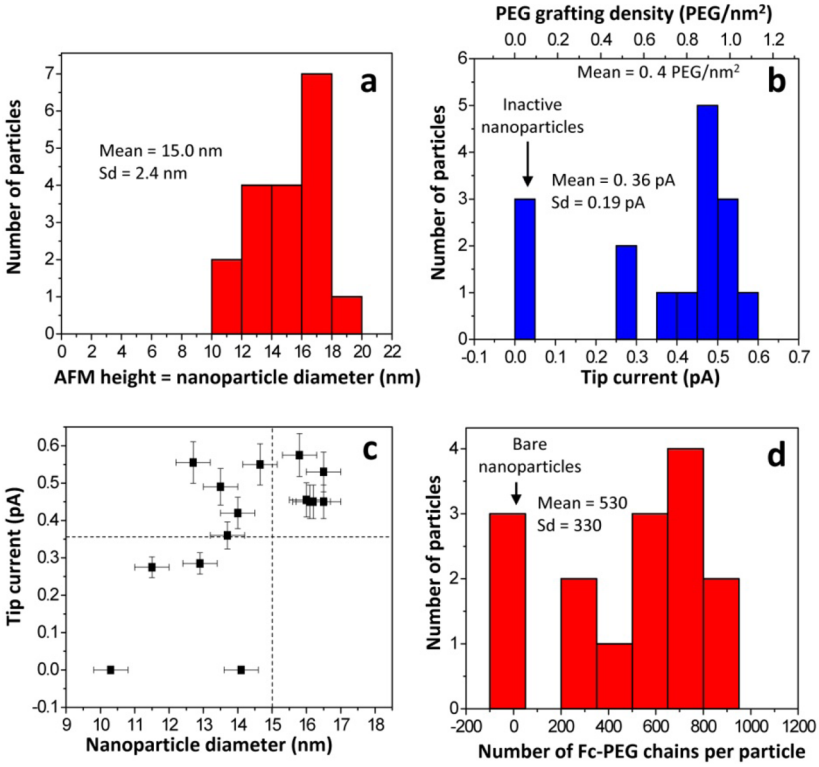

Figure 7. Statistical analysis of the properties of the Fc-PEGylated nanoparticles visible in the images presented in Figure 6. (a) Particle diameter histogram as derived from the topography image. (b) Tip current histogram, representing the distribution of the PEG coverage of the nanoparticles. (c) Attempt to cross-correlate the tip current with the nanoparticle size: The current generated by each particle is plotted as a function of its diameter. The horizontal and vertical dashed lines respectively indicate the average values of the tip current and nanoparticle diameter. (d) Histogram showing the distribution of the number of Fc-PEG chains per nanoparticle probed.

of the particles visible in the images reproduced in Figure 6, should be proportional to n_{av}, the average number of Fc-PEG chains per nanoparticle that we derived by cyclic voltametry, *i.e.*, $n_{av} = \pi\beta i d^2$. For the present case we find id^2= 150 pA nm^2 and n_{av} = 530, and we can thus derive the proportionality coefficient, β = 1.12 molecule nm^{-2}/pA, which allows the distribution of the $i_j\, d_j^2$ product to be converted into the actual distribution of chains per particle. This distribution is represented by the histogram shown in Figure 7d. One can see that among the nanoparticles probed most bear from 500 to 1000 chains, while a few did not bear any chains (*i.e.*, were apparently bare). Interestingly the histogram plot also shows that nanoparticles bearing as little as 200−300 Fc-PEG chains could electrochemically be detected by the tip. Finally, knowing the value of β also allows the tip current distribution to be converted into an explicit PEG grating density distribution (since $\Gamma_j = \beta i_j$), as shown in Figure 7b (upper abscissa). One can see that among the "active" particles many actually displayed a PEG grafting density close to 1 PEG/nm^2. This value is comparable to the grating density of ∼2 PEG/nm^2 reported for PEGylated gold nanoparticles free in solution, especially if one assumes that, because of nanoparticle immobilization, only the upper half of the nanoparticles was accessible for PEG grafting. However, because of the significant amount of particles either bare or displaying a low PEG grafting density, the average grafting density as derived from the distribution analysis is only ∼0.4 PEG/nm^2. We note that this value is compatible with our above estimate for the nanoparticle average grafting density (0.4−0.8 PEG/nm^2), which did not take into account the nanoparticle size distribution.

Even though the histograms presented above correspond to the analysis of a particular set of topographic and current images, similar analysis of several series of Mt/AFM-SECM images of different Fc-PEGylated nanoparticle arrays led to similar conclusions (see Supporting Information): as a result of a notable portion of particles remaining bare, the distribution of nanoparticle PEGylation encompassed values markedly higher than the average number of PEG chains per nanoparticle. We have no clear explanation for the consistently observed presence of these bare nanoparticles among the Fc-PEGylated particles. Yet we note that if the imaging conditions were altered so as to (over) decrease the average tip−surface distance, by increasing damping to >50%, a very intense short-circuit current was recorded at the level of these particles. Overall these results suggest that the surface of the inactive particles might actually bear a layer of

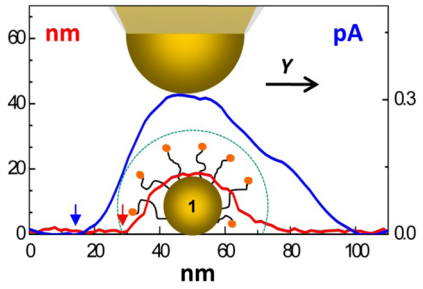

Figure 8. Illustration of how the Mt/AFM-SECM tip can selectively probe the PEG corona of Fc-PEGylated nanoparticles. The figure shows superimposed plots of the current (blue trace) and topography (red trace) signals measured along the vertical cross section of the corresponding images reproduced in Figure 6 and passing through the center of the nanoparticle labeled 1. The topography and current signals, the nanoparticle, and the idealized tip are represented to scale. The black arrow denotes the scan direction. The blue and red arrows denote the positions of the onsets of the current and topography signals. The PEG corona is represented by the green dotted circle. The shoulder on the right-hand side of the current peak is an artifact due to "tailing" of the current generated by a nearby nanoparticle (see Figure 6b).

molecular contaminants, which prevents Fc-PEG from grafting, but is nevertheless thin enough to allow the tip−nanoparticle electrical contact to occur. Likely candidates for such contaminants may be amine-thiol molecules that might have been transferred from the gold substrate to the nanoparticles by surface diffusion. We actually observed that replacing the amino-thiol SAM by an alkyl-dithiol SAM yielded a much larger percentage of "inactive" particles (data not shown). This result could be explained by the increased ability of alkyl-thiols, as opposed to amino-thiols, to efficiently surface-diffuse on gold.

Examining further the high-resolution Mt/AFM-SECM images presented in Figure 6 reveals another interesting phenomenon: Even if one considers only the direction perpendicular to the fast scan axis of the images (*i.e.*, the vertical direction), which is free of the current tailing effect discussed above, one can see that the current "spots" appear systematically broader than the corresponding nanoparticles. This trend can be better visualized by superimposing the vertical cross sections of the topograhy and current images taken along the particle labeled 1 in Figure 6, as shown in Figure 8.

Upon examining Figure 8, one can see that the current "peak" (blue trace) is indeed clearly broader than the topography peak (red trace). The tip of the AFM-SECM probe used to acquire the data, which as discussed above was characterized by an apparent radius of ~19 nm, is also represented schematically in Figure 8, at the same *scale* as the cross sections. The Fc-PEG coating of the particle, the so-called PEG corona, is represented as a hemisphere (green dotted line). This drawn-to-scale figure allows the origin of the differing width of the current and topographic peaks to be understood: one can see that when the probe is scanned laterally form left to right toward the nanoparticle, a current is detected at an onset position, marked by a blue arrow, where no topographic feature is detected. Only when the tip is moved further to the right is an onset of the topographic signal detected, at a position indicated by a red arrow, indicating that the tip then touches the gold nanoparticle itself. This difference in onset positions of the topographic and current signals is due to a phenomenon we observed previously when imaging Fc-PEG-functionalized band electrodes in tapping mode Mt/AFM-SECM:[41] because of the weak interactions between the tip and the PEG chains, the topography image reveals only the underlying grafting surface, whereas the tip current image shows a map of the surface distribution of Fc-PEG. Hence, in the present case, upon laterally approaching from a nanoparticle, the incoming tip first *selectively* probes electrochemically the corona of Fc-PEG chains before sensing the nanoparticle itself. The thickness of the Fc-PEG corona can thus be estimated from the difference in onset positions of the current and topography "peaks". From Figure 8 we find ~14 ± 2 nm for the corona thickness. This value is slightly larger than the distance of ~10 nm over which we have previously shown that Fc-PEG$_{3400}$ chains could shuttle electrons between a planar substrate and a tip. This result indicates that the Fc-PEG chains borne by the nanoparticles are indeed slightly elongated away from the nanoparticle surface, confirming that they form a dense "spherical brush". Another benefit of the differing specificity of the topography and electrochemical signals is that the nanoparticle dimensions can be measured from the topography image with no interference from the PEG coating.

CONCLUSION

We have demonstrated the possibility of probing individual Fc-PEGylated gold nanoparticles using Mt/AFM-SECM. We have shown that this original SECM-derived imaging technique affords the nanometer resolution required for resolving the position of *individual* nanoparticles and measuring their size, while simultaneously electrochemically interrogating the Fc-PEG chains they bear. The dual measurement of the size and current response of single nanoparticles uniquely allowed the statistical distribution in grafting density of PEG on the nanoparticles to be determined and correlated to the nanoparticle diameter. Moreover, because of its high spatial resolution and combined nature, Mt/AFM-SECM allowed "visualizing" simultaneously but independently the PEG corona and the gold core of individual nanoparticles. The present work indicates that nanoparticles functionalized by any kind of suitably redox-labeled biomacromolecules, such as short DNA strands or peptides, could be similarly characterized at the single-nanoparticle level by

Mt/AFM-SECM. Another perspective opened by the present work is that the use of nanoparticle arrays, such as those fabricated here, but involving nanoparticles only a few nanometers in size, *i.e.*, dimensionally close to biomacromolecules, should allow electrochemical measurements at the single-biomolecule level using Mt/AFM-SECM. Finally, we believe the present work is a clear example of the unique perspectives, in terms of revealing electrochemical (or electrochemically transduced) properties of individual nano-objects, offered by SECM-based techniques displaying a very high (*i.e.*, nanometer) resolution, first and foremost Mt/AFM-SECM.

METHODS

Chemicals. The linear [Fc-PEG_{3400}-S]$_2$-disulfide molecules (M_w = 7800; ~79 monomer units per chain) were custom-synthesized as described elsewhere.[59] 11-Amino-1-undecanethiol, $HS(CH_2)_{11}NH_2$ (99% purity), was purchased from Aldrich. Gold(III) chloride trihydrate ($HAuCl_4 \cdot 3H_2O$, ≥99.9% trace metals basis) from Aldrich and trisodium citrate (99% purity) from Alfa-Aesar were used for the synthesis of gold nanoparticles. All other chemicals and solvents were analytical grade and used without further purification. All aqueous solutions were made with Milli-Q purified water (Millipore).

Preparation of the Citrate-Stabilized Gold Nanoparticles. Citrate-stabilized AuNPs were prepared by the Frens method as reported in the literature (see Supporting Information).[60,61] The concentration of nanoparticles in the solution was 3 nM. The average particle size was checked by UV−vis spectra and SEM and AFM measurements and found to lie in the 15 to 20 nm range varying from batch to batch.

Preparation of the TS-Gold Surfaces. Flat gold surfaces were produced by template-stripping of a 200 nm thick gold layer deposited on mica,[62] as previously described.[43]

Assembly of the Random Fc-PEGylated Nanoparticle Array on the TS-Gold Surface. The freshly peeled TS-gold was immersed in a 1 mM solution of 11-amino-1-undecanethiol in ethanol for 48 h to allow the assembly of the NH_2-terminated SAM. The SAM-modified surface was then thoroughly rinsed with ethanol and left in this solvent for 10 min for desorption of weakly attached amino-thiol molecules if any. The surface was then carefully rinsed with Milli-Q (MQ) water and immersed into the nanoparticle solution. The immersion time in the nanoparticle solution was tuned so as to control the final coverage of the surface in nanoparticles. An immersion time of 30 min yielded a surface covered with a saturated layer of nanoparticles. This kind of surface was used to check the electrochemical response of 1,1′-ferrocene dimethanol at nanoparticle-covered surfaces by cyclic voltammetry (see Supporting Information). Decreasing the immersion time of the SAM-modified surface in the nanoparticle solution down to 1−10 min yielded surfaces with low to medium coverage in nanoparticles, which were further functionalized by Fc-PEG-disulfide as follows. After nanoparticle adsorption, the surface was rinsed with MQ water, mounted into a liquid cell, and covered with 200 μL of a 65 μM Fc-PEG-disulfide solution in MQ water. After a contact time ranging from 10 min to 1 h the surfaces was rinsed with water and the cell filled with the pH 6 0.1 M citrate buffer for characterization by cyclic voltammetry and Mt/AFM-SECM. Citrate buffer was chosen as the electrolyte solution because it was observed to yield the most reproducible results. We attribute this benefit to the fact that the buffer contains the nanoparticle capping agent, citrate, which may help stabilize the nanoparticle layer.

Fabrication and Pretreatment of the Combined AFM-SECM Tips. The tips were hand-fabricated according to a procedure adapted from the literature[63] and largely detailed elsewhere.[64] Briefly, a 60 μm diameter gold wire is flattened, and its extremity is successively bent and etched, so as to obtain a flexible cantilever (spring constant in the 0.5−3 N/m, fundamental flexural frequency ~2−3 kHz) bearing a conical tip with a spherical apex ~100 nm in radius. The etching process has been recently improved in order to reduce the tip radius down to ~20 nm (see Supporting Information). The tip is fully insulated by deposition of an electrophoretic paint and glued onto an AFM chip. The apex is selectively exposed in order to act as a current-sensing nanoelectrode. As a precaution against tip contamination, a monolayer of mercaptohexanol (MCH) was assembled on the exposed gold apex of the tip prior to AFM-SECM experiments. This MCH pretreatment was carried out by immersing the tip apex into a 1 mM MCH solution in aqueous solution for 2 h. The resulting MCH layer is thin enough to allow unhindered electron transfer of Fc heads to/from the tip, while greatly improving the tip durability.

AFM and Combined AFM-SECM Experiments. AFM images in air were acquired using a JPK microscope operated in tapping mode. The Mt/AFM-SECM experiments were carried out with a Molecular Imaging PICOSPM I AFM microscope (Agilent), which was modified as described in previous contributions (see Supporting Information).[41,59]

Cyclic Voltammetry. CV characterization of the gold surface bearing an array of Fc-PEGylated gold nanoparticles, at the various phases of its preparation, was carried out using the "substrate", low-sensitivity, channel of the homemade AFM-SECM bipotentiostat (see Supporting Information).

Conflict of Interest: The authors declare no competing financial interest.

Supporting Information Available: Experimental details and additional figures. This information is available free of charge *via* the Internet at http://pubs.acs.org.

Acknowledgment. The authors acknowledge the support of the French Agence Nationale de la Recherche (ANR) under reference ANR-09-PIRI-0005, "Cascade" project.

REFERENCES AND NOTES

1. *Metal Nanoparticles: Synthesis, Characterization, and Applications*; Feldheim, D. L., Foss, C. A., Eds.; Marcel Dekker: New York, 2002.
2. Sardar, R.; Funston, A. M.; Mulvaney, P.; Murray, R. W. Gold Nanoparticles: Past, Present, and Future. *Langmuir* **2009**, *25*, 13840–13851.
3. Daniel, M.-C.; Astruc, D. Gold Nanoparticles: Assembly, Supramolecular Chemistry, Quantum-Size-Related Properties, and Applications toward Biology, Catalysis, and Nanotechnology. *Chem. Rev.* **2004**, *104*, 293–346.
4. Saha, K.; Agasti, S. S.; Kim, C.; Li, X.; Rotello, V. M. Gold Nanoparticles in Chemical and Biological Sensing. *Chem. Rev.* **2012**, *112*, 2739–2779.
5. Elghanian, R.; Storhoff, J. J.; Mucic, R. C.; Letsinger, R. L.; Mirkin, C. A. Selective Colorimetric Detection of Polynucleotides Based on the Distance-Dependent Optical Properties of Gold Nanoparticles. *Science* **1997**, *277*, 1078–1081.
6. Rosi, N. L.; Mirkin, C. A. Nanostructures in Biodiagnostics. *Chem. Rev.* **2005**, *105*, 1547–1562.
7. Heitz, F.; Morris, M. C.; Divita, G. Twenty Years of Cell-Penetrating Peptides: From Molecular Mechanisms to Therapeutics. *Br. J. Pharmacol.* **2009**, *157*, 195–206.
8. Penn, S.; He, L.; Natan, M. Nanoparticles for Bioanalysis. *Curr. Opin. Chem. Biol.* **2003**, *7*, 609–615.
9. Jokers, J. V.; Lobovkina, T.; Zare, R. N.; Gambhir, S. S. Nanoparticle PEGylation for Imaging and Therapy. *Nanomedicine* **2011**, *6*, 715–728.
10. Wuelfing, W. P.; Gross, S. M.; Miles, D. T.; Murray, R. W. Nanometer Gold Clusters Protected by Surface-Bound Monolayers of Thiolated Poly(ethylene glycol) Polymer Electrolyte. *J. Am. Chem. Soc.* **1998**, *120*, 12696–12697.

11. Wolfe, R. L.; Balasubramanian, R.; Tracy, J. B.; Murray, R. W. Fully Ferrocenated Hexanethiolate Monolayer-Protected Gold Clusters. *Langmuir* **2007**, *23*, 2247–2254.
12. Murray, R. W. Nanoelectrochemistry: Metal Nanoparticles, Nanoelectrodes, and Nanopores. *Chem. Rev.* **2008**, *108*, 2688–2720.
13. Chow, K.-F.; Sardar, R.; Sassin, M. B; Wallace, J. M.; Feldberg, S. W.; Rolison, D. R.; Long, J. W.; Murray, R. W. 3D-Addressable Redox: Modifying Porous Carbon Electrodes with Ferrocenated 2 nm Gold Nanoparticles. *J. Phys. Chem. C* **2012**, *116*, 9283–9289.
14. Sardar, R.; Beasley, C. A.; Murray, R. W. Ferrocenated Au Nanoparticle Monolayer Adsorption on Self-Assembled Monolayer-Coated Electrodes. *Anal. Chem.* **2009**, *81*, 6960–6965.
15. McCarty, G. S.; Weiss, P. S. Scanning Probe Studies of Single Nanostructures. *Chem. Rev.* **1999**, *99*, 19683–1990.
16. Stiles, R. L.; Willets, K. A.; Sherry, L. J.; Roden, J. M.; Van Duyne, R. P. Investigating Tip-Nanoparticle Interactions in Spatially Correlated Total Internal Reflection Plasmon Spectroscopy and Atomic Force Microscopy. *J. Phys. Chem. C* **2008**, *112*, 11696–11701.
17. Gaiduk, A.; Yorulmaz, M.; Orrit, M. Correlated Absorption and Photoluminescence of Single Gold Nanoparticles. *ChemPhysChem* **2011**, *12*, 1536–1541.
18. Nuño, Z.; Hessler, B.; Ochoa, J.; Shon, Y.-S.; Bonney, C.; Abate, Y. Nanoscale Subsurface- and Material-Specific Identification of Single Nanoparticles. *Opt. Express* **2011**, *19*, 20865–20875.
19. Zachary Nuño, Z.; Hessler, B.; Heiberg, B.; Damato, R.; Dunlap, T.; Shon, Y.-S.; Abate, Y. Nanoscale Near-Field Infrared Spectroscopic Imaging of Silica-Shell/Gold-Core and Pure Silica Nanoparticles. *J. Nanopart. Res.* **2012**, *766*, 1–8.
20. Abate, Y.; Schwartzberg, A.; Strasser, D.; Leone, S. R. Nanometer-Scale Size Dependent Imaging of Cetyl Trimethyl Ammonium Bromide (CTAB) Capped and Uncapped Gold Nanoparticles by Apertureless Near-Field Optical Microscopy. *Chem. Phys. Lett.* **2009**, *474*, 146–152.
21. Bard, A. J. In *Scanning Electrochemical Microscopy*, second ed.; Bard, A. J., Mirkin, M. V., Eds.; Marcel Dekker: New York, 2012; pp 1−14.
22. Wittstock, G.; Burchardt, M.; Pust, E. S.; Shen, Y.; Zhao, C. Scanning Electrochemical Microscopy for Direct Imaging of Reaction Rates. *Angew. Chem., Int. Ed.* **2007**, *46*, 1584–1617.
23. Mirkin, M. V.; Nogala, W.; Velmurugan, J.; Wang, Y. Scanning Electrochemical Microscopy in The 21st Century. Update 1: Five Years After. *Phys. Chem. Chem. Phys.* **2011**, *13*, 21196–21212.
24. Tel-Vered, R.; Bard, A. J. Generation and Detection of Single Metal Nanoparticles Using Scanning Electrochemical Microscopy Techniques. *J. Phys. Chem. B* **2006**, *110*, 25279–25287.
25. Kueng, A.; Kranz, C.; Lugstein, A.; Bertagnolli, E.; Mizaikoff, B. Integrated AFM−SECM in Tapping Mode: Simultaneous Topographical and Electrochemical Imaging of Enzyme Activity. *Angew. Chem., Int. Ed.* **2003**, *42*, 3238–3240.
26. Kranz, C.; Kueng, A.; Lugstein, A.; Bertagnolli, E.; Mizaikoff, B. Mapping of Enzyme Activity by Detection of Enzymatic Products during AFM Imaging with Integrated SECM-AFM Probes. *Ultramicroscopy* **2004**, *100*, 127–134.
27. Hirata, Y.; Yabuki, S.; Mizutani, F. Application of Integrated SECM Ultra-Micro-Electrode and AFM Force Probe to Biosensor Surfaces. *Bioelectrochemistry* **2004**, *63*, 217–224.
28. Takahashi, Y.; Shevchuk, A. I.; Novak, P.; Murakami, Y.; Shiku, H.; Korchev, Y. E.; Matsue, T. Simultaneous Noncontact Topography and Electrochemical Imaging by SECM/SICM Featuring Ion Current Feedback Regulation. *J. Am. Chem. Soc.* **2010**, *132*, 10118–10126.
29. Etienne, M.; Anderson, E. C.; Evans, S. R.; Schuhmann, W.; Fritsch, I. Feedback-Independent Pt Nanoelectrodes for Shear Force-Based Constant-Distance Mode Scanning Electrochemical Microscopy. *Anal. Chem.* **2006**, *78*, 7317–7324.
30. Sun, P.; Mirkin, M. V. Kinetics of Electron-Transfer Reactions at Nanoelectrodes. *Anal. Chem.* **2006**, *78*, 6526–6534 and references therein.
31. Tel-Vered, R.; Walsh, D. A.; Mehrgardi, M. A.; Bard, A. J. Carbon Nanofiber Electrodes and Controlled Nanogaps for Scanning Electrochemical Microscopy Experiments. *Anal. Chem.* **2006**, *78*, 6959–6966.
32. Watkins, J. J.; Chen, J.; White, H. S.; Abruña, H. D.; Maisonhaute, E.; Amatore, C. Zeptomole Voltammetric Detection and Electron-Transfer Rate Measurements Using Platinum Electrodes of Nanometer Dimensions. *Anal. Chem.* **2003**, *75*, 3962–3971.
33. Xiong, H.; Gross, D. A.; Guo, J.; Amemiya, S. Local Feedback Mode of Scanning Electrochemical Microscopy for Electrochemical Characterization of One-Dimensional Nanostructure: Theory and Experiment with Nanoband Electrode as Model Substrate. *Anal. Chem.* **2006**, *78*, 1946–1957.
34. Kim, E.; Kim, J.; Amemiya, S. Spatially Resolved Detection of a Nanometer-Scale Gap by Scanning Electrochemical Microscopy. *Anal. Chem.* **2009**, *81*, 4788–4791.
35. Kim, J.; Xiong, H.; Hofmann, M.; Kong, J.; Amemiya, S. Scanning Electrochemical Microscopy of Individual Single-Walled Carbon Nanotubes. *Anal. Chem.* **2010**, *82*, 1605–1607.
36. Güella, A. G.; Ebejera, N.; Snowdena, M. E.; McKelveya, K.; Macpherson, J. V.; Unwin, P. R. Quantitative Nanoscale Visualization of Heterogeneous Electron Transfer Rates in 2D Carbon Nanotube Networks. *Proc. Natl. Acad. Sci. U.S.A.* **2012**, *109*, 11487–11492.
37. Lai, S. C. S.; Dudin, P. V.; Macpherson, J. V.; Unwin, P. R. Visualizing Zeptomole (Electro)Catalysis at Single Nanoparticles within an Ensemble. *J. Am. Chem. Soc.* **2011**, *133*, 10744–10747.
38. Ebejer, N.; Schnippering, M.; Colburn, A. W.; Edwards, M. A.; Unwin, P. R. Localized High Resolution Electrochemistry and Multifunctional Imaging: Scanning Electrochemical Cell Microscopy. *Anal. Chem.* **2010**, *82*, 9141–9145.
39. Kleijn, S. E. F.; Lai, S. C. S.; Miller, T. S.; Yanson, A. I.; Koper, M. T. M.; Unwin, P. R. Landing and Catalytic Characterization of Individual Nanoparticles on Electrode Surfaces. *J. Am. Chem. Soc.* **2012**, *134*, 18558–18561.
40. Meier, J.; Friedrich, K. A.; Stimming, U. Novel Method for the Investigation of Single Nanoparticle Reactivity. *Faraday Discuss.* **2002**, *121*, 365–372.
41. Abbou, A.; Anne, A.; Demaille, C. Probing the Structure and Dynamics of End-Grafted Flexible Polymer Chain Layers by Combined Atomic Force−Electrochemical Microscopy. Cyclic Voltammetry within Nanometer-Thick Macromolecular Poly(ethylene glycol) Layers. *J. Am. Chem. Soc.* **2004**, *126*, 10095–10108.
42. Abbou, J.; Anne, A.; Demaille, C. Accessing the Dynamics of End-Grafted Flexible Polymer Chains by Atomic Force-Electrochemical Microscopy. Theoretical Modeling of the Approach Curves by the Elastic Bounded Diffusion Model and Monte Carlo Simulations. Evidence for Compression-Induced Lateral Chain Escape. *J. Phys. Chem. B* **2006**, *110*, 22664–22675.
43. Anne, A.; Cambril, E.; Chovin, A.; Demaille, C. Touching Surface-Attached Molecules with a Microelectrode: Mapping the Distribution of Redox-Labeled Macromolecules by Electrochemical-Atomic Force Microscopy. *Anal. Chem.* **2010**, *82*, 6353–6362.
44. Anne, A.; Chovin, A.; Demaille, C.; Lafouresse, M. High-Resolution Mapping of Redox-Immunomarked Proteins Using Electrochemical Atomic Force Microscopy in Molecule Touching Mode. *Anal. Chem.* **2011**, *83*, 7924–7932.
45. Wang, K.; Goyer, C.; Anne, A.; Demaille, C. Exploring the Motional Dynamics of End-Grafted DNA Oligonucleotides by in *Situ* Electrochemical Atomic Force Microscopy. *J. Phys. Chem. B* **2007**, *111*, 6051–6058.
46. Xia, X.; Yang, M.; Wang, Y.; Zheng, Y.; Li, Q.; Chen, J.; C; Xia, Y. Quantifying the Coverage Density of Poly(ethylene glycol) Chains on the Surface of Gold Nanostructures. *ACS Nano* **2012**, *6*, 512–522.
47. Benoit, D. N.; Huiguang, Z.; Lilierose, M. H.; Verm, R. A.; Ali, N.; Morrison, A. N.; Fortner, J. D.; Avendano, C.; Colvin, V. L. Measuring the Grafting Density of Nanoparticles in Solution by Analytical Ultracentrifugation and Total Organic Carbon Analysis. *Anal. Chem.* **2012**, *84*, 9238–9245.

48. Shein, J. B.; Lai, L. M. H.; Eggers, P. K.; Paddon-Row, M. N.; Gooding, J. J. Formation of Efficient Electron Transfer Pathways by Adsorbing Gold Nanoparticles to Self-Assembled Monolayer Modified Electrodes. *Langmuir* **2009**, *25*, 11121–11128.
49. Dyne, J.; Lin, Y.-S.; Lai, L. M. H.; Ginges, J. Z.; Luais, E.; Peterson, J. R.; Goon, I. Y.; Amal, R.; Gooding, J. J. Some More Observations on the Unique Electrochemical Properties of Electrode-Monolayer-Nanoparticle Constructs. *ChemPhysChem* **2010**, *11*, 2807–2813.
50. Grabar, K. C.; Allison, K. J.; Baker, B. E.; Bright, R. M.; Brown, K. R.; Freeman, R. G.; Fox, A. P.; Keating, C. D.; Musick, M. D.; Natan, M. J. Two-Dimensional Arrays of Colloidal Gold Particles: A Flexible Approach to Macroscopic Metal Surfaces. *Langmuir* **1996**, *12*, 2353–2361.
51. Bethell, D.; Brust, M.; Schiffrin, D. J.; Kiely, C. From Monolayers to Nanostructured Materials: an Organic Chemist's View of Self-Assembly. *J. Electroanal. Chem.* **1996**, *409*, 137–143.
52. Kissling, G. P.; Miles, D. O.; Fermín, D. J. Electrochemical Charge Transfer Mediated by Metal Nanoparticles and Quantum Dots. *Phys. Chem. Chem. Phys.* **2011**, *13*, 21175–21185.
53. Chazalviel, J.-N.; Allongue, P. On the Origin of the Efficient Nanoparticle Mediated Electron Transfer across a Self-Assembled Monolayer. *J. Am. Chem. Soc.* **2011**, *133*, 762–764.
54. Laviron, E. The Use of Linear Potential Sweep Voltammetry and of a.c. Voltammetry for the Study of the Surface Electrochemical Reaction of Strongly Adsorbed Systems and of Redox Modified Electrodes. *J. Electroanal. Chem.* **1979**, *100*, 263–270.
55. Daoud, M.; Cotton, J. P. Star Shaped Polymers: A Model for the Conformation and its Concentration Dependence. *J. Phys. (Paris)* **1982**, *43*, 531–538.
56. Ball, R. C.; Marko, J. F.; Milner, S. T.; Witten, T. A. Polymers Grafted to a Convex Surface. *Macromolecules* **1991**, *24*, 693–703.
57. Binder, K.; Milchev, A. Polymer Brushes on Flat and Curved Surfaces: How Computer Simulations Can Help to Test Theories and to Interpret Experiments. *J. Polym. Sci., Part B: Polym. Phys.* **2012**, *50*, 1515–1555.
58. Grabar, K. C.; Brown, K. R.; Keating, C. D.; Stranick, S. J.; Tang, S.-L.; Natan, M. J. Nanoscale Characterization of Gold Colloid Monolayers: A Comparison of Four Techniques. *Anal. Chem.* **1997**, *69*, 471–477.
59. Anne, A.; Demaille, C.; Goyer, C. Electrochemical Atomic-Force Microscopy Using a Tip-Attached Redox Mediator. Proof-of-Concept and Perspectives for Functional Probing of Nanosystems. *ACS Nano* **2009**, *3*, 819–827.
60. Frens, G. Controlled Nucleation for the Regulation of the Particle Size in Monodisperse Gold Suspensions. *Nat. Phys. Sci.* **1973**, *241*, 20–22.
61. Nath, N.; Chilkoti, A. Label-Free Biosensing by Surface Plasmon Resonance of Nanoparticles on Glass: Optimization of Nanoparticle Size. *Anal. Chem.* **2004**, *76*, 5370–5378.
62. Hegner, M.; Wagner, P.; Semenza, G. Ultralarge Atomically Flat Template-Stripped Au Surfaces for Scanning Probe Microscopy. *Surf. Sci.* **1993**, *291*, 39–46.
63. Macpherson, J. V.; Unwin, P. R. Combined Scanning Electrochemical−Atomic Force Microscopy. *Anal. Chem.* **2000**, *72*, 276–285.
64. Abbou, J.; Demaille, C.; Druet, M.; Moiroux, J. Fabrication of Submicrometer-Sized Gold Electrodes of Controlled Geometry for Scanning Electrochemical-Atomic Force Microscopy. *Anal. Chem.* **2002**, *74*, 6355–6363.